THE JOURNAL OF PHYSICAL CHEMISTRY Letters

Letter

pubs.acs.org/JPCL

Homogeneous Emission Line Broadening in the Organo Lead Halide Perovskite $CH_3NH_3PbI_{3-x}Cl_x$

Christian Wehrenfennig, Mingzhen Liu, Henry J. Snaith, Michael B. Johnston, and Laura M. Herz*

University of Oxford, Department of Physics, Clarendon Laboratory, Parks Road, Oxford OX1 3PU, United Kingdom

Supporting Information

ABSTRACT: The organic–inorganic hybrid perovskites methylammonium lead iodide ($CH_3NH_3PbI_3$) and the partially chlorine-substituted mixed halide $CH_3NH_3PbI_{3-x}Cl_x$ emit strong and broad photoluminescence (PL) around their band gap energy of ∼1.6 eV. However, the nature of the radiative decay channels behind the observed emission and, in particular, the spectral broadening mechanisms are still unclear. Here we investigate these processes for high-quality vapor-deposited films of $CH_3NH_3PbI_{3-x}Cl_x$ using time- and excitation-energy dependent photoluminescence spectroscopy. We show that the PL spectrum is homogenously broadened with a line width of 103 meV most likely as a consequence of phonon coupling effects. Further analysis reveals that defects or trap states play a minor role in radiative decay channels. In terms of possible lasing applications, the emission spectrum of the perovskite is sufficiently broad to have potential for amplification of light pulses below 100 fs pulse duration.

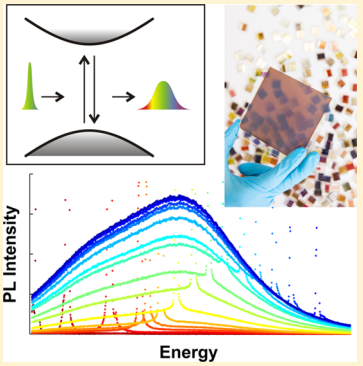

SECTION: Energy Conversion and Storage; Energy and Charge Transport

Organometal halide perovskites have recently created a surge of attention following their impressive performance in thin-film solar cells.[1−4] A major advantage of these organic–inorganic hybrid materials is their ability to combine the favorable properties of inorganic semiconductors – especially their high carrier mobilities[5−7] – with the flexibility and low-temperature processability of organic materials. Organometal halide perovskites have already been studied to some extent over the past two decades,[5,8−10] when the main applications targeted were thin-film transistors and light-emitting diodes. Research efforts penetrated the whole breadth of the material class, encompassing fully confined and 2-D layered structures that exhibited high tunablility of their excitonic properties via the size of the organic cationic molecule.[11] More recently, the main focus has been on 3-D materials in the classic perovskite configuration ABX_3, where the cation A is a small organic molecule such as methylammonium or formamidinium, B is a metal, and X a halogen. In particular, high-quality methylammonium lead iodide ($CH_3NH_3PbI_3$) and the mixed halide obtained by partial substitution with chlorine ($CH_3NH_3PbI_{3-x}Cl_x$) have been successfully used in high-efficiency solar cells,[3,4] where they exhibit favorable optical and electronic properties such as strong optical absorption in the visible and ultraviolet spectrum,[2] long free charge carrier lifetimes, and high carrier mobilities.[7,12−14] These properties are also highly desirable for many other optoelectronic applications, where organic–inorganic perovskites could once more lead to a step change in feasibility or performance. However, little in-depth knowledge exists to date on what governs the behavior of the emissive species in these materials.

In this work, we investigate the intense, broad band-edge luminescence from $CH_3NH_3PbI_{3-x}Cl_x$ with the intention of unravelling the nature of the emission line broadening and the underlying radiative recombination processes. We focus on thin films fabricated from thermal vapor deposition, which allows for smooth film-formation and high crystalline order, making them very suitable for general device applications.[4] Using photoluminescence spectroscopy with continuously tunable excitation energy, we scrutinize the broadening mechanism in the mixed halide $CH_3NH_3PbI_{3-x}Cl_x$, which features an emission peak around its band-gap energy (1.62 eV) with a full width at half-maximum (FWHM) of 103 meV. By scanning the excitation energy across the width of this peak while observing the spectral shape of the PL emission, we establish that the spectral broadening is homogeneous. We further acquire time-resolved emission spectra and find that the spectral shape is invariant between 200 ps and 200 ns after excitation, suggesting an absence of significant disorder-related effects in the emissive species. On the basis of our observations, we propose strong phonon coupling of charge carriers arising from their polaronic properties as a likely source of the homogeneous broadening. Owing to the uncertainty relation between pulse duration and frequency bandwidth manifested in the natural spectral line width, a broad emission spectrum is one of the primary prerequisites for gain materials in ultrashort (femtosecond) pulsed lasers.[15] Here perovskites could also offer a perspective for electrically pumped designs creating a significant advantage over many well-established femtosecond-laser gain materials that require optical pumping. With the observed spectral width

Received: February 28, 2014
Accepted: March 24, 2014
Published: March 24, 2014

 © 2014 American Chemical Society

of 103 meV, the homogeneous gain medium could sustain amplification of light pulses as short as 6.4 fs.

Figure 1a displays the optical transmission and reflection spectra of a vapor-deposited $CH_3NH_3PbI_{3-x}Cl_x$ film in the

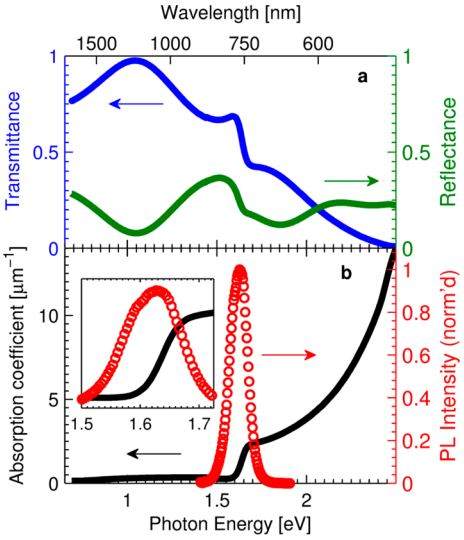

Figure 1. (a) Optical transmittance ($T_{ext} = I_{transmitted}/I_{incident}$, blue) and reflectance spectra ($R = I_{reflected}/I_{incident}$, green) of evaporated films of $CH_3NH_3PbI_{3-x}Cl_x$. T was determined in specular transmission geometry and R in specular reflection geometry at close to normal (6°) incidence. (b) Black curve: absorption coefficient $\alpha = -1/d \ln(T_{ext}/(1 - R))$, calculated from the data in panel a and the film's thickness d = 330 nm (black). Red circles: Photoluminescence emission spectrum at 1.96 eV excitation energy (λ = 634 nm), 6 μJ/cm^2 fluence, and 2 MHz repetition rate. Inset: magnification of the plot in the energy range around the absorption edge and PL emission.

NIR/VIS range. The onset of interband absorption can be identified as an edge centered at 1.64 eV, in agreement with previously published data on thin films of solution-processed mixed halide $CH_3NH_3PbI_{3-x}Cl_x$ (refs 2, 6, and 12) and trihalide $CH_3NH_3PbI_3$ (ref 16) materials. At photon energies below the steep absorption onset at 1.64 eV, the transmission and reflectance spectra exhibit clear thin-film-interference (Fabry–Perot) effects, which indicates that the film thickness is very uniform and the surface is optically flat, preventing any substantial light scattering. From the data in Figure 1a and the film thickness d = 330 nm (determined from SEM cross sectional imaging), we obtain the absorption coefficient shown in Figure 1b together with the PL emission spectrum. Because information on excitonic effects is still emerging and the exact nature of the electronic structure near the band edge is still being explored, extraction of the precise band gap energy is difficult due to the lack of an unambiguous physical description of the absorption onset. A direct semiconductor in accordance with the results of band-structure calculations[17−20] ought to exhibit a broad regime for which $\alpha \propto (E - E_g)^{1/2}$ near the absorption onset.[21] Such a square-root behavior would at best partially fit the initial steep rise around 1.64 eV, leaving the following sharp transition to a flatter regime difficult to account for. Absorption enhancements at the band edge caused by resonant exciton creation would provide a plausible explanation for an initially steeper rise of the absorption coefficient.[22] Exciton binding energies have been reported for the pure halide $CH_3NH_3PbI_3$ to range from 20 meV (ref 23) to 37 meV (ref 24), which is sufficiently high for enhancement effects to be observed at room temperature, given that for T = 297 K the characteristic thermal energy is k_BT = 25.6 meV. We note that reliable clarification of the nature of the absorption onset may require in-depth theoretical modeling, for example, in conjunction with low-temperature absorption data to allow isolation of individual contributions.

The photoluminescence emission spectrum of vapor-deposited $CH_3NH_3PbI_{3-x}Cl_x$ is shown along with the absorption data in Figure 1b. We find that the spectrum has a full width at half-maximum (FWHM) of 103 meV. With its center of mass (1.617 eV) near the low-energy tail of the absorption edge, the PL emission appears to show a slight down-shift in energy with respect to the band gap. The magnitude of any potential shift is, however, subject to some uncertainty due to the previously mentioned ambiguities in the precise location of the band gap energy. Such Stokes shifts are commonly observed in different materials for a variety of reasons including migration of excitations to low-energy sites[25] and lattice relaxation (polaronic effects).[26,27] More remarkable is the apparent presence of additional broadening mechanisms, resulting in the emission line width being almost twice as broad as the spectral width of the absorption onset (56 meV, determined as the FWHM of the derivative of the absorption edge; see Supporting Information).

To probe the mechanisms that underlie the broadening of the PL emission spectrum, we recorded photoluminescence spectra while scanning the excitation energy through the absorption edge and across the full range of the emission spectrum. For this experiment, we operated the Ti:sapphire pump laser in continuous wave mode to allow spectrally narrow excitation of the sample. A representative subset of the acquired spectra is shown in Figure 2a. Because it is experimentally impossible to fully separate scattered excitation light from the photoluminescence, the spectra also exhibit additional sharp peaks at the corresponding excitation energy. In Figure 2b, we plot the spectrally integrated PL emission intensity as a function of excitation energy. For this purpose, the PL intensity was normalized for excitation photon flux and the scattered excitation light peaks were removed through data interpolation.

From the excitation energy-dependent PL data, we can make the striking observation that across the entire excitation range the emission spectrum has an identical shape. While this result is visually apparent from the spectra shown in Figure 2a, we provide further analysis by extracting the energy of maximum emission and the positions of the left and right half-maxima as a function of excitation energy in Figure 2b (see also normalized spectra in Supporting Information). While the uncertainty increases in the regime of weaker PL emission (as indicated by the error bars), Figure 2b confirms that the emission spectrum of $CH_3NH_3PbI_{3-x}Cl_x$ is independent of excitation energy across the interband absorption onset. We therefore conclude that the broadening mechanism must be homogeneous; that is, the emission at every single site is itself equally and fully broadened. If this were not the case, selective excitation within a distribution of inhomogeneous sites would generate charge pairs only at those sites that are tuned to the particular excitation energy used. As a result, the excitation energy would be site-selective, and the emission spectra would shift to reflect the local nature of the sites selected. Such site-selective emission shifts can, for example, be observed for thin films of disordered polymeric semiconductors exhibiting significant inhomogeneous spectral broadening.[25] In contrast, our observation of shape-persistent emission spectra for resonant

dx.doi.org/10.1021/jz500434p | J. Phys. Chem. Lett. 2014, 5, 1300−1306

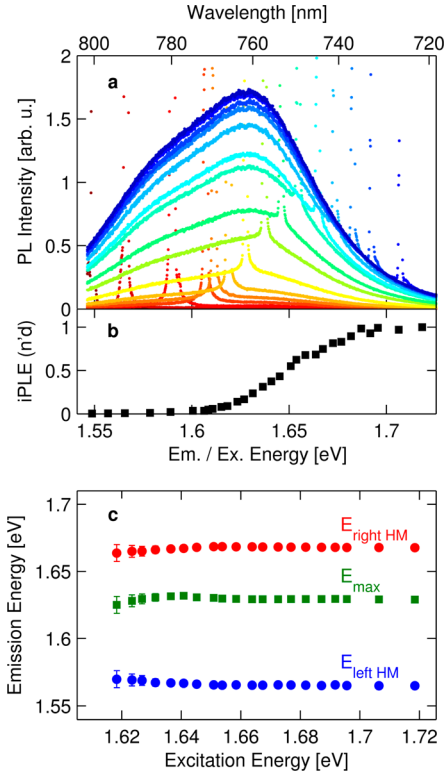

Figure 2. (a) PL emission spectra of evaporated $CH_3NH_3PbI_{3-x}Cl_x$ films on glass (PL intensity vs. emission energy), taken at excitation energies close to the absorption edge ranging from 1.55 eV (dark red) to 1.73 eV (dark blue). The excitation intensity was held constant at 5 W cm^{-2}. The narrow peaks originate from scattered excitation light and can be used as a visual indicator of the excitation energy. (b) Spectrally integrated PL intensity as a function of excitation energy for evaporated films of $CH_3NH_3PbI_{3-x}Cl_x$ as extracted from the data shown in panel a. (c) Energy of the PL emission maximum extracted from the data shown in panel a plotted against excitation energy (green squares). The energies at which the emission reaches half its maximum intensity are shown as red and blue circles.

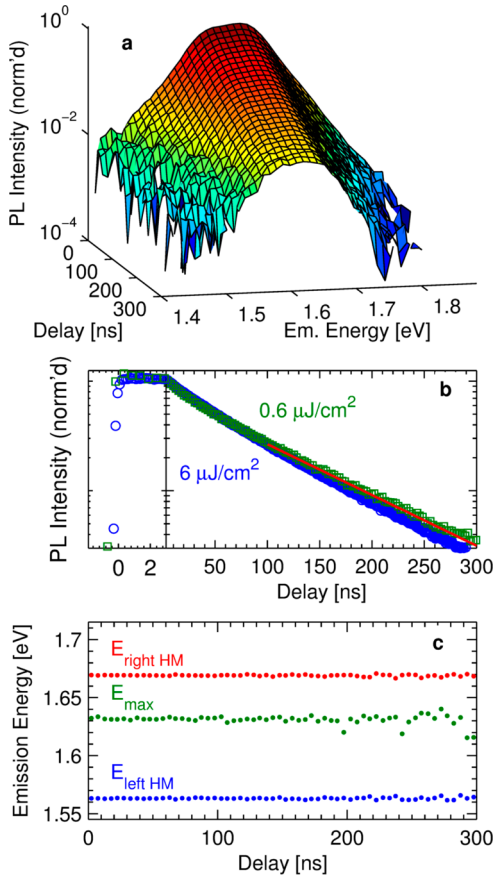

Figure 3. (a) 3D representation of the time-resolved PL emission spectrum of evaporated $CH_3NH_3PbI_{3-x}Cl_x$ acquired by means of time-correlated single photon counting at various emission energies (excitation energy: 1.96 eV, fluence: 6 $\mu J/cm^2$, repetition rate: 2 MHz.) (b) Time-resolved PL emission decay at the spectral maximum for excitation fluences of 6 and 0.6 $\mu J/cm^2$ acquired in the same way as the data in panel a. Red line: fit of a monoexponential decay function to the low-fluence data for the time-delay interval from 100 to 300 ns. The resulting decay time constant is (94.2 ± 0.9) ns with $\chi_{red}^2 = 1.04$. (c) Photon energy at the emission maximum (green) and the energies at which the emission reaches half its maximum intensity (red and blue) as extracted from the data shown in panel a, plotted against the time delay between excitation and emission.

excitation throughout the emission spectrum of vapor-deposited $CH_3NH_3PbI_{3-x}Cl_x$ highlights the low degree of disorder present in these thin films.

To gain further insights into the dynamics of radiative decay channels in $CH_3NH_3PbI_{3-x}Cl_x$ and the factors determining the spectral shape of the emission, we recorded time-resolved photoluminescence spectra by means of time-correlated single photon counting (TCSPC). PL decay traces were recorded for a range of regularly spaced emission energies and the spectra at the desired time-delays reconstructed from the data. Figure 3a shows the resulting 3-D plot of the emission spectra at various times after pulsed excitation at 2.43 eV. Visual inspection of these data reveals an essentially time-independent spectral shape of the PL emission. (See Supporting Information for normalized spectra.) Again, we extract the energetic positions of the emission maximum and half-intensity points of each spectrum to allow for better inspection of potential changes in the spectrum over time. (See Figure 3c.) This plot clearly confirms that the PL emission spectrum of $CH_3NH_3PbI_{3-x}Cl_x$ is time-independent for time delays between 200 ps and 200 ns. Again, these results suggest an absence of significant inhomogeneous broadening arising from energetic disorder. For materials incorporating a broad energetic distribution of sites, as for example semiconducting polymer films,[28,29] porous silicon,[30] or heavily doped crystalline GaAs,[31] pulsed excitation of the material is usually followed by gradual emission shifts toward lower energy with time, resulting from migration to lower energy sites in the inhomogeneous distribution. The absence of such emission energy shifts with time after excitation in $CH_3NH_3PbI_{3-x}Cl_x$ films is therefore fully compatible with our prior observation of a predominantly homogeneously broadened emission line width.

Figure 3b shows that the PL emission intensity from vapor-deposited $CH_3NH_3PbI_{3-x}Cl_x$ decays relatively slowly over a few 100 ns after excitation, in similarity to previous reports[12,13] for solution-processed films. The observed PL transients are almost fully monoexponential and only exhibit very slightly increasing decay rates for increased excitation fluences. As previously reported for solution-processed $CH_3NH_3PbI_{3-x}Cl_x$ films, such effects arise mainly from the onset of bimolecular charge recombination, which becomes more and more dominant as the charge-carrier density is increased.[7] From the PL decay at low excitation fluence (0.6 $\mu J/cm^2$) and at longer delays (>100

dx.doi.org/10.1021/jz500434p | J. Phys. Chem. Lett. 2014, 5, 1300−1306

ns) after excitation, a monomolecular decay lifetime of 94 ns can be extracted by fitting a single exponential decay function to the data. We also note that while there is some fluence-dependence of the PL decay rate, the shape of the emission spectra was found to be independent of excitation fluence for values up to at least 20 $\mu J/cm^2$ (not shown). This observation again suggests an absence of disorder-related effects such as potential saturation of low-energy states in the tail of an inhomogeneously broadened density of states that would induce spectral shifts with increasing excitation fluence.

For the discussion of our findings, we consider several processes that can potentially cause substantial homogeneous PL emission broadening and the observed asymmetry with the spectral broadening of the absorption edge. The simplest origin of homogeneous broadening is given by the natural line width of $\Delta E = \hbar/\tau$ caused by the finite lifetime τ of the excited state.[15] The observed asymmetry between absorption and emission broadening would in this case require at least one additional intermediate state in the recombination process with an extremely short lifetime $\leq$6.4 fs (corresponding to ΔE = 103 meV), which is six orders of magnitude shorter than the overall decay dynamics we actually observe in time-resolved PL (Figure 3c). In addition, lifetime broadening would have to result in a Lorentzian emission line shape;[15] however, the observed spectra (Figure 2a), and, in particular, the shape of the tails that resemble those of a Gaussian, are not consistent with a Lorentzian distribution function. We therefore conclude that lifetime broadening is not responsible for the dominant contribution to the observed broad emission line width.

Another possible source of homogeneous broadening lies in the participation of phonons in the radiative recombination process. Figure 2a clearly shows that the PL emission spectra feature a superposition of at least two peaks. It appears that a possible underlying composition could consist of a band-edge emission peak and a number of side bands responsible for the shoulder at ~1.58 eV and the broad tails. PL side-bands are commonly found to arise from phonon creation or annihilation and have been observed in a whole variety of materials, ranging from inorganic semiconductors such as silicon[32] and colloidal nanocrystals[33−36] to metal halides[37−39] and organic (molecular) semiconductors.[25] We have recently shown that the low-frequency photoconductivity spectra of solution-processed $CH_3NH_3PbI_{3-x}Cl_x$ and $CH_3NH_3PbI_3$ films contain the signature of metal halide lattice vibrations.[7] It therefore seems likely that the emission from such photogenerated charge pairs is also subject to interaction with phonons. Given the large size of the crystallites for these vapor-deposited films of $CH_3NH_3PbI_{3-x}Cl_x$ (extending to hundreds of nanometers; see ref 4) and the absence of time-dependent spectral emission features, the phonon coupling mechanism will most likely arise directly from the intrinsic nature of the bulk material rather then derive from surface-mediated effects. In further support for the presence of such vibrational effects, we show the changes in absorption edge and PL emission spectra for temperature lower than 297 K (see Supporting Information). For the absorption edge, a sharpening compatible with a reduction in thermal broadening is observed at 160 K. For the PL emission, the high-energy edge sharpens at 160 K, as would be expected for reduced phonon absorption at lower temperature. The low-energy edge still shows a side shoulder, in agreement with phonon emission, which ought to be largely unaffected by temperature. Hence these results underline the notion of phonon coupling contributing to the emission from this material.

In the picture of electronic band structure, processes involving phonon creation or annihilation simultaneous to the emission of the photon are of particular importance in indirect gap semiconductors, where a third particle is needed during electron−hole recombination to accept the momentum difference between conduction band minimum (CBM) and valence band maximum (VBM). Luminescence from indirect semiconductors hence often exhibits a broadened spectrum, as for example, observed in crystalline silicon.[32] Band structure calculations have so far postulated a direct band gap for the methylammonium lead halides $CH_3NH_3PbI_3$ (refs 17−20), $CH_3NH_3PbCl_3$ (ref 19), and $CH_3NH_3PbI_{3-x}Cl_x$ (ref 19). Similar recombination dynamics to those in indirect semiconductors could, however, also arise from the existence of a second conduction band valley that is only separated from the main (Γ-) valley by a low-energy barrier, allowing rapid equilibration of their populations. The low bimolecular decay rates and the observation of Auger processes in $CH_3NH_3PbI_{3-x}Cl_x$ (refs 7, 12, and 13) suggest that recombination via the direct transition is in some way inhibited, which leaves the possibility for an additional indirect transition to become a dominant recombination pathway. We note however that the likelihood of this scenario to apply in the present case is reduced by the fact that calculations of the electronic band structure of $CH_3NH_3PbI_{3-x}Cl_x$ have so far not indicated the presence of a second valley.[19]

As an alternative concept, the observed broadening may be attributed to polaronic effects, similar to those observed in molecular semiconductors[40,41] or metal halides.[39] Here the photogenerated electron−hole pair strongly couples to the underlying lattice, which leads to a geometric lattice relaxation around the created charge. As a result, the emission is found to be Stokes-shifted from the absorption edge and likely contains phonon features. For materials with strongly ionic bonding and hence strong exciton−phonon interaction, Coulomb-correlated electron−hole pairs have therefore also been referred to as "self-trapped excitons".[39] Such phenomena have been evoked in alkali halides,[42] transition-metal halides,[38] and also certain perovskites.[43,44] They are therefore likely to also play a role in the related compounds here. We note that for metal halides the barrier to self-trapping was found to be generally low, and the process appeared to occur on ultrashort (subpicosecond) time scales related to the involved lattice vibration periods.[39] We therefore would not necessarily expect any signature of self-trapping dynamics in the time-resolved PL spectra shown in Figure 3a, as these were taken with much lower time-resolution. Previous work on alkali halides often revealed significant Stokes shifts between absorption and emission.[39] For the $CH_3NH_3PbI_{3-x}Cl_x$ films under investigation here, the lack of an unambiguous physical decomposition of the broad absorption and emission features prevents the extraction of an exact Stokes shift. However by visual inspection of Figure 1b, we find that possible values could at most be on the order of 30 meV. This suggests that any polaronic effects in this system are comparatively small, in agreement with the high charge-carrier mobilities[7] and long diffusion lengths[12−14] recently reported for solution-processed methylammonium lead halide perovskite films. Hence while polaronic effects may be present in these materials, they appear to be sufficiently small to still allow excellent charge extraction and high open-circuit voltages

dx.doi.org/10.1021/jz500434p | J. Phys. Chem. Lett. 2014, 5, 1300−1306

in planar-heterojunction photovoltaic device architectures.[4,7,12−14]

Our observation of a strongly homogeneously broadened emission line shape has two implications for device applications. First, the absence of spectral shifts resulting, for example, from site-selective excitation or excitation migration in these materials suggests that disorder and trapping is scarce, at least for the dominant bulk-like emissive species. This finding again highlights the suitability of these materials for photovoltaic applications, for which material disorder in systems such as organic semiconductors, mesoporous metal oxides, and amorphous silicon has been shown to correlate with a reduction in photovoltage.[45] We cannot rule out the presence of disorder or traps near the surfaces of the perovskite, as these contribute little to the overall emission in terms of volume fraction. However, surface states are also highly accessible to passivation treatments[46,47] that can be more easily applied here than throughout the bulk structure. Second, materials with broad homogeneous emission line shapes fulfill a central requirement for gain media in femtosecond lasers due to the high natural bandwidth of ultrashort pulses (103 meV at 6.4 fs). Organolead halide perovskites already show many of the required properties for lasing operation, such as strong emission and a sufficiently long-lived upper state. The potential for electrical injection due to the good charge conductivity of the material[6,7] may create a crucial advantage over existing gain media, enabling more compact and efficient laser systems than those relying on optical pumping.

In conclusion, we have investigated the origin of spectral broadening in the emission of vapor-deposited $CH_3NH_3PbI_{3-x}Cl_x$. By recording PL spectra while continuously tuning the excitation energy across the spectral range of the emission peak, we reveal that no observable selective excitation occurs of subsites in resonance with the respective energy. We hence establish that the broadening mechanism is homogeneous with an associated width of 103 meV. We furthermore show that the PL emission spectrum does not exhibit a dependence on time after excitation or excitation fluence, suggesting a high degree of order present in the film. The slightly Stokes-shifted and homogenously broadened PL spectra exhibit features consistent with phonon coupling as the dominant spectral broadening mechanism of the emission from $CH_3NH_3PbI_{3-x}Cl_x$. Our findings underline the potential of organometal halide perovskites for a wider range of optoelectronic applications beyond photovoltaic energy conversion. In particular, the observed broad homogeneous line width ought to allow amplification of Fourier-transform-limited pulses with sub-100 fs duration, making these materials interesting for pulsed laser operation.

EXPERIMENTAL METHODS

Sample Preparation. Thin films of $CH_3NH_3PbI_{3-x}Cl_x$ perovskite were deposited by dual-source evaporation, as described in detail in ref 4. Lead chloride ($PbCl_2$) and methylammonium iodide (CH_3NH_3I) were deposited simultaneously onto 1.7 mm thick glass substrates under high vacuum. Before starting the evaporation, the tooling factor (which is a ratio of the material deposited on the sensors to that on the samples) was estimated for each source individually.

Approximately 500 mg of CH_3NH_3I and 100 mg of $PbCl_2$ were loaded into separate crucibles, and the substrates were placed in a substrate holder above the sources. The two crucibles were heated above the desired deposition temperatures under high vacuum (10^{-5} mbar) for ∼5 min to eliminate volatile impurities in the chamber before coating the substrates with perovskite. To prepare representative perovskite films, we set key deposition parameters such as the deposition rates and duration for the two sources as previously optimized for best performance of the material in solar cells.[4] This includes using a CH_3NH_3I:$PbCl_2$ molar ratio of 4:1 and deposition rates of 5.3 Å s^{-1} for CH_3NH_3I (crucible temperature around 116 °C) and 1 Å s^{-1} for $PbCl_2$ (crucible temperature of around 320 °C), maintained for ∼128 min of evaporation. The substrate holder was rotated to ensure uniform coating, while the film was deposited on the substrate. Annealing the as-deposited films at 100 °C for 45 min in a N_2-filled glovebox enabled full crystallization of the perovskite, darkening the color and resulting in an apparent growth of crystal features visible in SEM images.[4] The resulting film thickness is 330 ± 5 nm.

Photoluminescence Spectroscopy. Photoluminescence spectroscopy with continuously tunable excitation is performed using an experimental setup based on a tunable Ti:sapphire laser operated in continuous-wave mode. A variable attenuator is used to stabilize the intensity incident on the sample at ∼5 W cm^{-2} across the full photon energy range. Samples are mounted in a vacuum cell maintaining a pressure below 10^{-5} mbar. In this environment, the materials are observed to be stable over days involving exposure to the excitation light for many hours, with no degradation in PL or visual change in film appearance observed for the duration of the measurements. Photoluminescence from the sample is collected by a pair of off-axis parabolic mirrors and focused onto the entry slit of a grating monochromator. Polarizers in the excitation and emission beam path ensure that only luminescence of perpendicular polarization to the excitation light is detected to suppress scattered excitation light. Entry slit width and grating constant of the monochromator are chosen to achieve a spectral resolution $\Delta\lambda$ better than 0.5 nm. The spectrally resolved PL is detected by a nitrogen-cooled Si-CCD detector and corrected for spectral response of the apparatus by using a tungsten filament lamp of known emissivity spectrum. Unless otherwise stated, measurements were taken at room temperature (297 K).

Time-Resolved Photoluminescence. Time-resolved photoluminescence experiments are performed on a PicoQuant FluoTime 300 fluorescence spectrometer by means of time-correlated single-photon counting. A pulsed diode laser operating at a photon energy of 1.96 eV (634 nm) excites the sample, which is contained in a vacuum chamber at pressures below 10^{-5} mbar, with a repetition rate of 2 MHz. PL is collected through a lens and detected at perpendicular polarization with respect to the excitation light. A grating monochromator is configured to provide spectral filtering with a resolution $\Delta\lambda$ of ∼2 nm before photons are counted by a hybrid photodetector. A variable attenuator in the emission path is used to ensure counting rates are kept below 1% of the repetition rate to avoid multiphoton events. All measurements were taken at room temperature (297 K).

Optical Absorption Spectra. Optical absorption spectra were acquired in a Perkin-Elmer Lambda 1050 UV/vis/NIR spectrophotometer with spectral resolution of 2 nm.

ASSOCIATED CONTENT

Supporting Information

Derivative of the absorption coefficient. Normalized plots of PL emission spectra. Low-temperature PL emission and optical

dx.doi.org/10.1021/jz500434p | J. Phys. Chem. Lett. 2014, 5, 1300−1306

absorption spectra. This material is available free of charge via the Internet at http://pubs.acs.org.

AUTHOR INFORMATION

Corresponding Author

*E-mail: l.herz@physics.ox.ac.uk.

Notes

The authors declare no competing financial interests.

ACKNOWLEDGMENTS

We gratefully acknowledge funding from the Engineering and Physical Sciences Research Council.

REFERENCES

(1) Kim, H.-S.; Lee, C.-R.; Im, J.-H.; Lee, K.-B.; Moehl, T.; Marchioro, A.; Moon, S.-J.; Humphry-Baker, R.; Yum, J.-H.; Moser, J. E.; et al. Lead Iodide Perovskite Sensitized All-Solid-State Submicron Thin Film Mesoscopic Solar Cell with Efficiency Exceeding 9%. *Sci. Rep.* **2012**, *2*, 591.

(2) Lee, M. M.; Teuscher, J.; Miyasaka, T.; Murakami, T. N.; Snaith, H. J. Efficient Hybrid Solar Cells Based on Meso-Superstructured Organometal Halide Perovskites. *Science* **2012**, *338*, 643−647.

(3) Burschka, J.; Pellet, N.; Moon, S.-J.; Humphry-Baker, R.; Gao, P.; Nazeeruddin, M. K.; Gratzel, M. Sequential Deposition as a Route to High-Performance Perovskite-Sensitized Solar Cells. *Nature* **2013**, *499*, 316−319.

(4) Liu, M.; Johnston, M. B.; Snaith, H. J. Efficient Planar Heterojunction Perovskite Solar Cells by Vapour Deposition. *Nature* **2013**, *501*, 395−398.

(5) Mitzi, D. B.; Feild, C. A.; Schlesinger, Z.; Laibowitz, R. B. Transport, Optical, and Magnetic Properties of the Conducting Halide Perovskite $CH_3NH_3SnI_3$. *J. Solid State Chem.* **1995**, *114*, 159−163.

(6) Stoumpos, C. C.; Malliakas, C. D.; Kanatzidis, M. G. Semiconducting Tin and Lead Iodide Perovskites with Organic Cations: Phase Transitions, High Mobilities, and Near-Infrared Photoluminescent Properties. *Inorg. Chem.* **2013**, *52*, 9019−9038.

(7) Wehrenfennig, C.; Eperon, G. E.; Johnston, M. B.; Snaith, H. J.; Herz, L. M. High Charge Carrier Mobilities and Lifetimes in Organolead Trihalide Perovskites. *Adv. Mater.* **2014**, *26*, 1584−1589.

(8) Chondroudis, K.; Mitzi, D. B. Electroluminescence from an Organic−Inorganic Perovskite Incorporating a Quaterthiophene Dye within Lead Halide Perovskite Layers. *Chem. Mater.* **1999**, *11*, 3028−3030.

(9) Mitzi, D. B.; Chondroudis, K.; Kagan, C. R. Organic-Inorganic Electronics. *IBM J. Res. Dev.* **2001**, *45*, 29−45.

(10) Mitzi, D. B. Synthesis, Structure, and Properties of Organic-Inorganic Perovskites and Related Materials. In *Prog. Inorg. Chem.*; John Wiley & Sons: Hoboken, NJ, 2007; Chapter 1, pp 1−121.

(11) Papavassiliou, G. C.; Koutselas, I. B. Structural, Optical and Related Properties of Some Natural 3-Dimensional and Lower-Dimensional Semiconductor Systems. *Synth. Met.* **1995**, *71*, 1713−1714.

(12) Stranks, S. D.; Eperon, G. E.; Grancini, G.; Menelaou, C.; Alcocer, M. J. P.; Leijtens, T.; Herz, L. M.; Petrozza, A.; Snaith, H. J. Electron-Hole Diffusion Lengths Exceeding 1 Micrometer in an Organometal Trihalide Perovskite Absorber. *Science* **2013**, *342*, 341−344.

(13) Xing, G.; Mathews, N.; Sun, S.; Lim, S. S.; Lam, Y. M.; Grätzel, M.; Mhaisalkar, S.; Sum, T. C. Long-Range Balanced Electron- and Hole-Transport Lengths in Organic-Inorganic $CH_3NH_3PbI_3$. *Science* **2013**, *342*, 344−347.

(14) Gonzalez-Pedro, V.; Juárez-Pérez, E. J.; Arsyad, W. S.; Barea, E. M.; Fabregat-Santiago, F.; Mora-Sero, I.; Bisquert, J. General Working Principles of $CH_3NH_3PbX_3$ Perovskite Solar Cells. *Nano Lett.* **2014**, *14*, 888−893.

(15) Svelto, O. *Principles of Lasers*; Springer: New York, 2010.

(16) Cai, B.; Xing, Y.; Yang, Z.; Zhang, W.-H.; Qiu, J. High Performance Hybrid Solar Cells Sensitized by Organolead Halide Perovskites. *Energy Environ. Sci.* **2013**, *6*, 1480−1485.

(17) Koutselas, I. B.; Ducasse, L.; Papavassiliou, G. C. Electronic Properties of Three- and Low-Dimensional Semiconducting Materials with Pb Halide and Sn halide Units. *J. Phys.: Condens. Matter* **1996**, *8*, 1217.

(18) Umebayashi, T.; Asai, K.; Kondo, T.; Nakao, A. Electronic Structures of Lead Iodide Based Low-Dimensional Crystals. *Phys. Rev. B* **2003**, *67*, 155405.

(19) Mosconi, E.; Amat, A.; Nazeeruddin, M. K.; Grätzel, M.; De Angelis, F. First Principles Modeling of Mixed Halide Organometal Perovskites for Photovoltaic Applications. *J. Phys. Chem. C* **2013**, *117*, 13902−13913.

(20) Even, J.; Pedesseau, L.; Jancu, J.-M.; Katan, C. Importance of Spin−Orbit Coupling in Hybrid Organic/Inorganic Perovskites for Photovoltaic Applications. *J. Phys. Chem. Lett.* **2013**, *4*, 2999−3005.

(21) Fox, M. *Optical Properties of Solids*, 2nd ed.; Oxford University Press: New York, 2010.

(22) Sturge, M. D. Optical Absorption of Gallium Arsenide between 0.6 and 2.75 eV. *Phys. Rev.* **1962**, *127*, 768−773.

(23) Sun, S.; Salim, T.; Mathews, N.; Duchamp, M.; Boothroyd, C.; Xing, G.; Sum, T. C.; Lam, Y. M. The Origin of High Efficiency in Low-Temperature Solution-Processable Bilayer Organometal Halide Hybrid Solar Cells. *Energy Environ. Sci.* **2014**, *7*, 339−407.

(24) Hirasawa, M.; Ishihara, T.; Goto, T.; Uchida, K.; Miura, N. Magnetoabsorption of the Lowest Exciton in Perovskite-Type Compound $(CH_3NH_3)PbI_3$. *Physica B* **1994**, *201*, 427−430.

(25) Bässler, H.; Schweitzer, B. Site-Selective Fluorescence Spectroscopy of Conjugated Polymers and Oligomers. *Acc. Chem. Res.* **1999**, *32*, 173−182.

(26) Pope, M.; Swenberg, C. E. *Electronic Processes in Organic Crystals and Polymers*; Oxford Science: New York, 1999.

(27) Pelant, I.; Valenta, J. *Luminescence Spectroscopy of Semiconductors*; Oxford University Press: New York, 2012.

(28) Meskers, S. C. J.; Hübner, J.; Oestreich, M.; Bässler, H. Dispersive Relaxation Dynamics of Photoexcitations in a Polyfluorene Film Involving Energy Transfer: Experiment and Monte Carlo Simulations. *J. Phys. Chem. B* **2001**, *105*, 9139−9149.

(29) Herz, L. M.; Silva, C.; Grimsdale, A. C.; Müllen, K.; Phillips, R. T. Time-Dependent Energy Transfer Rates in a Conjugated Polymer Guest-Host System. *Phys. Rev. B* **2004**, *70*, 165207.

(30) Song, L.; El-Sayed, M. A.; Chen, P. C. Spectral Diffusion within the Porous Silicon Emission Wavelength Range on the Nanosecond to Millisecond Time Scale. *J. Appl. Phys.* **1997**, *82*, 836−839.

(31) Göbel, E. O.; Graudszus, W. Optical Detection of Multiple-Trapping Relaxation in Disordered Crystalline Semiconductors. *Phys. Rev. Lett.* **1982**, *48*, 1277−1280.

(32) Haynes, J. R.; Lax, M.; Flood, W. F. Analysis of Intrinsic Recombination Radiation from Silicon and Germanium. *J. Phys. Chem. Solids* **1959**, *8*, 392−396.

(33) Sagar, D. M.; Cooney, R. R.; Sewall, S. L.; Dias, E. A.; Barsan, M. M.; Butler, I. S.; Kambhampati, P. Size Dependent, State-Resolved Studies of Exciton-Phonon Couplings in Strongly Confined Semiconductor Quantum Dots. *Phys. Rev. B* **2008**, *77*, 235321.

(34) Kambhampati, P. Unraveling the Structure and Dynamics of Excitons in Semiconductor Quantum Dots. *Acc. Chem. Res.* **2011**, *44*, 1.

(35) Mooney, J.; Krause, M. M.; Saari, J. I.; Kambhampati, P. A Microscopic Picture of Surface Charge Trapping in Semiconductor Nanocrystals. *J. Chem. Phys.* **2013**, *138*, 204705.

(36) Mooney, J.; Krause, M. M.; Saari, J. I.; Kambhampati, P. Challenge to the Deep-Trap Model of the Surface in Semiconductor Nanocrystals. *Phys. Rev. B* **2013**, *87*, 081201(R).

(37) Ikehara, T.; Itoh, T. Dynamical Behavior of the Exciton Polariton in CuCl: Coherent Propagation and Momentum Relaxation. *Phys. Rev. B* **1991**, *44*, 9283−9294.

(38) von der Osten, W.; Stolz, H. Localized Exciton States in Silver Halides. *J. Phys. Chem. Solids* **1990**, *51*, 765−791.

(39) Williams, R. T.; Song, K. S. The Self-Trapped Exciton. *J. Phys. Chem. Solids* **1990**, *51*, 679−716.
(40) Heeger, A. J.; Kivelson, S.; Schrieffer, J. R.; Su, W. P. Solitons in Conducting Polymers. *Rev. Mod. Phys.* **1988**, *60*, 781−850.
(41) Furukawa, M.; Mizuno, K.-i.; Matsui, A.; D. D. V. Rughooputh, S.; C. Walker, W. Time-Resolved Excitonic Luminescence Processes in Poly(phenylenevinylene). *J. Phys. Soc. Jpn.* **1989**, *58*, 2976−2987.
(42) Känzig, W. Electron Spin Resonance of V1-Centers. *Phys. Rev.* **1955**, *99*, 1890−1891.
(43) Lewis, J. T.; Kolopus, J. L.; Sonder, E.; Abraham, M. M. Reorientation and Motion of the Self-Trapped Hole in $KMgF_3$. *Phys. Rev. B* **1973**, *7*, 810−818.
(44) Tale, I.; Springis, M.; Rogulis, U.; Ogorodnik, V.; Kulis, P.; Tale, V.; Veispals, A.; Fitting, H.-J. Self-Trapped Holes and Recombination Luminescence in $LiBaF_3$ Crystals. *Radiat. Meas.* **2001**, *33*, 751−754.
(45) Nayak, P. K.; Garcia-Belmonte, G.; Kahn, A.; Bisquert, J.; Cahen, D. Photovoltaic Efficiency Limits and Material Disorder. *Energy Environ. Sci.* **2012**, *5*, 6022−6039.
(46) Tiwana, P.; Parkinson, P.; Johnston, M. B.; Snaith, H. J.; Herz, L. M. Ultrafast Terahertz Conductivity Dynamics in Mesoporous TiO2: Influence of Dye Sensitization and Surface Treatment in Solid-State Dye-Sensitized Solar Cells. *J. Phys. Chem. C* **2010**, *114*, 1365−1371.
(47) Tiwana, P.; Docampo, P.; Johnston, M. B.; Herz, L. M.; Snaith, H. J. The Origin of an Efficiency Improving "Light Soaking" Effect in SnO2 Based Solid-State Dye-Sensitized Solar Cells. *Energy Environ. Sci.* **2012**, *5*, 9566−9573.

■ NOTE ADDED AFTER ASAP PUBLICATION

This Letter was published ASAP on March 27, 2014, with an incorrect value for the lifetime τ throughout. The corrected version was reposted on April 17, 2014.